Catalysis Science & Technology

PAPER

View Article Online
View Journal

Published on 16 June 2017. Downloaded by University of Science and Technology of China on 03/07/2017 14:06:55.

Check for updates

Cite this: DOI: 10.1039/c7cy00706j

First-principles study of structure sensitivity of chain growth and selectivity in Fischer–Tropsch synthesis using HCP cobalt catalysts†

Hai-Yan Su, [a] Yonghui Zhao,[b] Jin-Xun Liu,[a] Keju Sun *[c] and Wei-Xue Li *[ad]

Received 11th April 2017,
Accepted 30th May 2017

DOI: 10.1039/c7cy00706j

rsc.li/catalysis

Structure sensitivity on chain growth and selectivity in cobalt catalyzed Fischer–Tropsch synthesis (FTS) were studied by density functional theory (DFT) calculations. It is found that at a lower CO coverage, chain growth tends to proceed *via* a CO insertion mechanism on close-packed Co (0001) and stepped Co, with CH_4 as the main product. However, a carbide mechanism is preferable on more open Co (10$\bar{1}$1) accompanied with higher selectivity to C_2 hydrocarbons than CH_4. The origin is identified from the structure sensitive adsorption of the key intermediates, specifically the least "saturated" C/CH species, which exhibit a relatively strong dependence on the structure evolution. With increasing CO coverage, the CO insertion mechanism becomes more favorable, and both FTS activity and C_2 hydrocarbon selectivity increase on Co (0001). This work highlights the intrinsic structure and coverage effects, achieving fundamental insight that can potentially be used to design and develop improved catalysts for FTS and other important reactions in syngas conversion.

Introduction

Fischer–Tropsch synthesis (FTS), which converts synthesis gas (a mixture of CO and H_2), produced from coal, natural gas or biomass, to high molecular weight hydrocarbons, provides alternative fuel to that derived from crude oil.[1–3] The reaction is initiated by CO activation *via* either a direct or H-assisted pathway, leading to the formation of CH_x species.[4–10] The CH_x species generated then undergoes a surface-catalyzed stepwise polymerization process by "C_1" monomers. To date, two primary chain growth mechanistic proposals exist, and they differ with each other in the source of "C_1" monomers: from CH_x (carbide mechanism) or CO (CO insertion mechanism).[11–36] For the carbide mechanism, the "CH_2" intermediate is commonly believed to be the key chain building unit experimentally, which disagrees with most of the theoretical studies due to its low surface concentration, and instead the "CH" intermediate has been suggested to be more related. Compared to the carbide mechanism, the CO insertion mechanism, which includes a number of oxygenate intermediates in addition to hydrocarbon intermediates, is more complicated and less elucidated. The investigations of all the intermediates and elementary reaction pathways are demanding, and a simplification for the CO insertion process is much needed but currently unavailable. Methanation is a main competing pathway to chain growth, and the overall efficiency for FTS requires catalysts with high chain growth probability but low selectivity to methane.

The catalyst structure and reaction conditions have also been demonstrated to have a dramatic influence on FTS,[37–49] in addition to the complexity in the reaction process. It has been suggested that the catalyst activity and selectivity are a strong function of the particle size when the size of the metal particle falls in the range of a few nanometers.[39–44] The origin for the particle size effect remains in debate, which has been assigned to the decrease in the number of B_5 active sites, the blocking of edge/corner by CO or oxidization of metallic cobalt with decreasing particle size. For larger particles (10–210 nm), such structure sensitivity has not been observed.[45] Besides the particle size, the catalytic performance also depends significantly on the crystal phase of the metal.[46–48] For instance, hexagonal close-packed (HCP) Co

[a] State Key Laboratory of Molecular Reaction Dynamics, State Key Laboratory of Catalysis, Dalian Institute of Chemical Physics, Chinese Academy of Science, Dalian 116023, China
[b] CAS Key Laboratory of Low-Carbon Conversion Science and Engineering, Shanghai Advanced Research Institute, Chinese Academy of Science, Shanghai 201203, China
[c] Key Laboratory of Applied Chemistry, College of Environmental and Chemical Engineering, Yanshan University, Qinhuangdao 066004, China. E-mail: kjsun@ysu.edu.cn
[d] Department of Chemical Physics, College of Chemistry and Materials Science, Hefei National Laboratory for Physical Sciences at the Microscale, iChEM, CAS Center for Excellence in Nanoscience, University of Science and Technology of China, Hefei 230026, China. E-mail: wxli70@ustc.edu.cn

† Electronic supplementary information (ESI) available: Energetics and structures for various intermediates' adsorption; energetics and transition state structures for CO insertion, CH_x (x = 0–3) coupling and hydrogenation reactions on Co (0001), stepped Co and Co (10$\bar{1}$1). See DOI: 10.1039/c7cy00706j

Published on 16 June 2017. Downloaded by University of Science and Technology of China on 03/07/2017 14:06:55.

catalysts have presented higher activity than face centered-cubic (FCC) Co catalysts.[46,47] Based on a first-principles kinetic study, we found that CO activation on HCP Co not only has much higher intrinsic activity than that of FCC Co but also prefers a different reaction route, direct dissociation *versus* H-assisted dissociation.[6] The origin is identified from the formation of various denser yet favorable active sites on HCP Co not available for FCC Co, due to their distinct crystallographic structure and morphology. Interestingly, the crystal phase effect is quite different for different metals. Recently, combined with theoretical analysis, material synthesis and characterization, we have shown that water-dispersible fcc Ru catalysts containing abundant open facets have a mass-specific activity of at least three times higher than the previous best hcp Ru catalysts in the aqueous-phase FTS.[48] The origin of the higher mass-specific activity of the fcc Ru catalysts is identified experimentally from the 2 orders of magnitude higher density of the active sites, despite their slightly higher apparent barrier. These studies on the structure–performance relation indicate that three surface structures, including (0001), stepped sites and open surfaces are the possible active sites for FTS. In addition, the reaction conditions, such as temperature, pressure, H_2/CO ratio *etc.*, also greatly affect reaction activity and selectivity.[39,45,49] Taking account of all the factors from the catalytic reaction, surface structure and reaction conditions (coverage) in FTS still represents a significant challenge.

Herein, we introduce a density functional theory (DFT)-based simplification of the FTS process that combines the formation free energy (G_{FORM}) and activity of C–O bond scission assessments for 19 possible C_2-oxygenate intermediates to identify the key intermediates and minimum energy pathways for the first C–C bond formation *via* the CO insertion mechanism, which is subsequently compared with the carbide mechanism and methanation. We have focused on the currently proposed active sites for FTS in the literatures, namely Co (0001), stepped Co and Co (10$\bar{1}$1) (represents the open Co surface),[6,9,17,18,45,50] and employed high coverage of the $\left(2\sqrt{3}\times 2\sqrt{3}\right)$R30°-CO structure ($\theta_{CO}$ = 7/12 ML) reported by low-energy electron diffraction (LEED) and high-pressure infrared reflection absorption spectroscopy (RAIRS) experiments to better simulate real reaction conditions (Fig. 1).[51,52] The intrinsic structure and coverage effects on the chain growth mechanism and selectivity and their link with atomic-scale properties are identified.

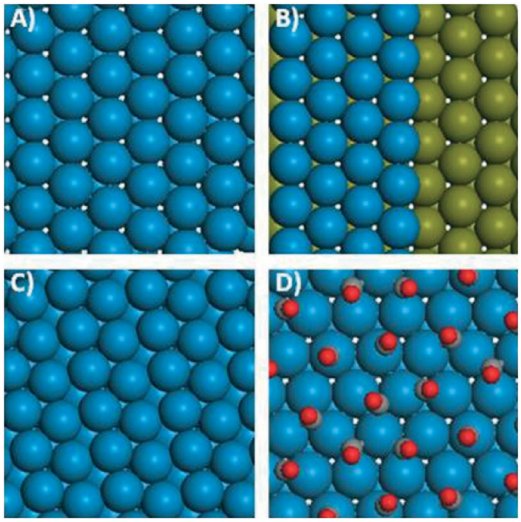

Fig. 1 The schematic structures (top view) of the (A) Co (0001) (B) stepped Co, (C) Co (10$\bar{1}$1) and (D) $\left(2\sqrt{3}\times 2\sqrt{3}\right)$R30° CO/Co (0001) surface. The blue, dark yellow, grey and red balls represent upper Co, lower Co, C and O atoms, respectively.

Methods

Spin-polarized DFT calculations were performed using the Vienna *Ab initio* Simulation Package (VASP).[53] The interaction between the ionic cores and electrons was described by the projector-augmented wave (PAW) method, and the Kohn–Sham valence electronic wavefunction was expanded in a plane-wave basis set with a kinetic energy cutoff at 400 eV. The exchange–correlation effects were represented within the generalized gradient approximation (GGA) using the Perdew–Burke–Ernzerhof (PBE) exchange–correlation functional.[54] The energies were converged to within 10^{-4} eV per atom, and the forces were converged to within 0.03 eV Å^{-1}.

The Co (0001) and Co (10$\bar{1}$1) surfaces were modeled using a four-layer slab within (3 × 3) and (2 × 2) surface unit cells, respectively. We calculated the adsorption of C_2-oxygenate intermediates in the (3 × 2) unit cell on Co (10$\bar{1}$1), and found a difference in the adsorption energy compared to the corresponding results in the (2 × 2) unit cell to be within the accuracy of our calculations. Thus, the (2 × 2) unit cell is sufficient for Co (10$\bar{1}$1). The stepped Co surface was modeled using a four-layer (7 × 3) close-packed surface, in which three neighboring rows of metal atoms on the top layer are removed. A vacuum region of 15 Å between any two repeated slabs was found to be sufficient to avoid interactions between repeated slabs along the *z*-direction. The surface Brillouin zone was sampled with (4 × 4 × 1), (5 × 5 × 1) and (4 × 2 × 1) Monkhorst–Pack *k*-point grid meshes for the Co (0001), Co (10$\bar{1}$1) and stepped Co surfaces, respectively.[55] The top two layers and the adsorbates were fully relaxed, and the remaining layers were fixed in their bulk truncated positions. The lattice constants for hexagonal bulk cobalt were calculated to be $a = b$ = 2.50 Å, c = 4.03 Å, in good agreement with the experimental values ($a = b$ = 2.51 Å, c = 4.06 Å).

All transition states (TSs) were located by the force reversed method[56] and the climbing-image nudged elastic band method (CI-NEB).[57] The relaxation will stop until the residual forces in each atom were smaller than 0.03 eV Å^{-1}. The elementary activation barrier was calculated with respect to the most stable state for separate adsorption of adsorbates on the surfaces, unless otherwise indicated.

This journal is © The Royal Society of Chemistry 2017

Published on 16 June 2017. Downloaded by University of Science and Technology of China on 03/07/2017 14:06:55.

The calculated formation free energies (G_{FORM}) of the C_2-oxygenate intermediates C_2H_xO are defined as the reaction free energies of the following reaction:

$$2CO(g) + 3H_2(g) + (8 - x)^* \rightarrow C_2H_xO^* + O^* + (6 - x)H^* \quad (1)$$

where CO and H_2 are in the gas phase, $C_2H_xO^*$, O* and H* are the adsorbed species on the surfaces, and * are the clean surfaces. The calculated G_{FORM} values for the C_2-oxygenate intermediates are obtained by evaluating the free-energy differences between the subsystems involved in the reaction (1) as follows:

$$G_{FORM} = G_{C_2HxO^*} + G_{O^*} + (6 - x)G_{H^*} - 2G_{CO(g)} - 3G_{H_2(g)} - (8 - x)G^* \quad (2)$$

where G is the free-energy of each subsystem involved in the reaction (1). For slab and adsorbed species, we neglect the entropy (S) effect. The G for the gas-phase species is obtained by $G = E_{TOTAL} - TS + RT\ln(P/P^0)$, where E_{TOTAL} is the energy of the gas-phase species, S is the entropy at temperature T, P and P^0 are the partial pressure of gas-phase species and the standard pressure, respectively. In this article, typical FTS conditions on Co-based catalysts (500 K, 2 MPa, $H_2/CO = 2:1$) are employed.[45] The more negative the G_{FORM}, the higher the concentrations of intermediates are at equilibrium conditions.[58] Zero point energy corrections are not included.

Results and discussion

Effect of the surface structure on Fischer–Tropsch synthesis

CO insertion mechanism on Co (0001) and stepped Co. The CO insertion mechanism starts with CO insertion of CH_x (x = 0–3) and proceeds *via* C–O bond scission, followed by hydrogenation or *vice versa*.[28–36] In a previous work, we present a HCO insertion chain growth mechanism.[34] Because of the similarity between HCO and CO insertion mechanisms, we mainly focus on the CO insertion mechanism for the first C–C bond formation below. In this mechanism, there are 19 possible C_2-oxygenate intermediates in total, and the investigations of all possible intermediates and elementary pathways are demanding. We can simplify this problem considerably by introducing the formation free energies (G_{FORM}, see the Computational methods section) and activation energies (E_{ACT}) of C–O bond scission for 19 C_2-oxygenate intermediates, as illustrated in Fig. 2A and B. To achieve a high chain growth probability, the C_2-oxygenate intermediates should be facile to be produced (G_{FORM} as negative as possible) and decomposed (E_{ACT} as small as possible).

The 19 possible C_2-oxygenate intermediates can be generally divided into two types: alcohols or aldehydes/ketones, depending on whether the O end attaches an H atom or not (see structures in Fig. S1 and S2 and adsorption energies E_{ADS} in Table S1†). As shown in Fig. 2A and B, the alcohol intermediates primarily focus on region I where G_{FORM} is more positive on Co (0001) (>−0.58 eV) and stepped Co (>−1.33 eV), whereas the aldehyde/ketone intermediates fall in regions II and III with more exothermic G_{FORM} values (<−0.58 and −1.33 eV). The insert in Fig. 2A shows that the alcohol intermediates bind with the surface only through their C ends, whereas most of the aldehyde/ketone intermediates bind with the surface through both C and O ends, thereby leading to their stronger binding with the surfaces. The possible reason for the different adsorption configurations is that O in alcohol intermediates can be considered to be "saturated", and thus no unpaired p electrons are available to bind with the surface, in contrast with O in aldehyde/ketone intermediates. The unfavorable adsorption configurations of the alcohol intermediates not only lead to their lower equilibrium concentrations but inhibit subsequent C–O bond cleavage. Therefore, the alcohol intermediates that mostly fall in region I are excluded as the possible precursors for the CO insertion mechanism. Additionally, several quasi-aldehyde intermediates, namely CH_xCH_2O (x = 1–3), are also excluded due to either more positive G_{FORM} or an undesirable binding mode

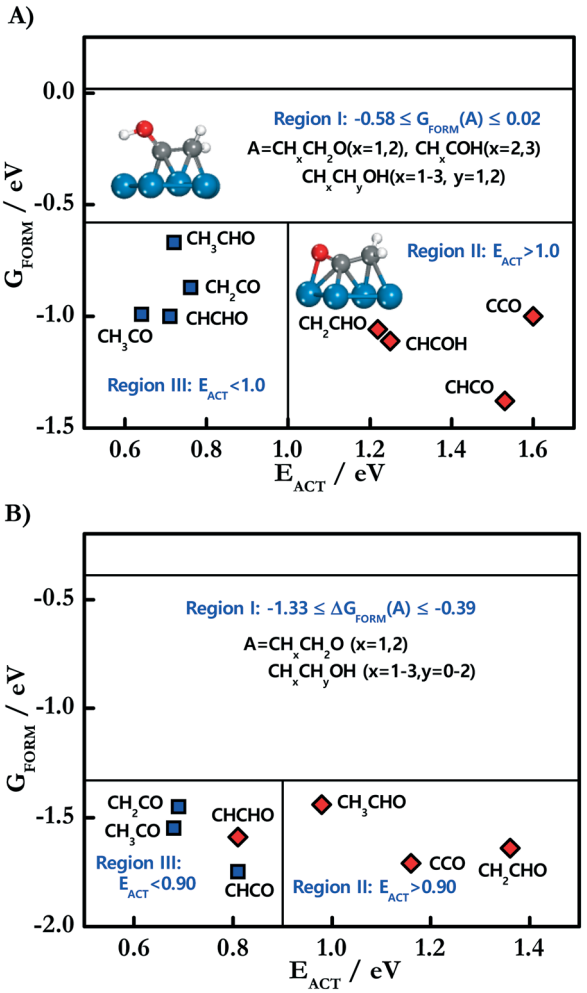

Fig. 2 Formation free energies G_{FORM} (with respect to gaseous CO, H_2 and clean surfaces) of C_2-oxygenate intermediates plotted as a function of their activation energies E_{ACT} for C–O bond scission on (A) Co (0001) and (B) stepped Co.

Published on 16 June 2017. Downloaded by University of Science and Technology of China on 03/07/2017 14:06:55.

(only O binds with the surface in CH_3CH_2O) for subsequent C–O bond cleavage.

For the remaining 7–8 C_2-oxygenate intermediates, we calculate their activation energies (E_{ACT}) for C-O bond scission on Co (0001) and stepped Co, as shown in regions II and III in Fig. 2A and B (see TS structures in Fig. 3). It can be seen that four intermediates fall in the region of interest (region III), which have much smaller E_{ACT} (0.64–0.76 eV for Co (0001), 0.68–0.81 eV for stepped Co, see Table S2†) than region II. CHCHO and CH_xCO (x = 2, 3) appear in region III on both Co (0001) and stepped Co. The CH_2CO intermediate has recently been detected as a key intermediate in CO hydrogenation by synchrotron-based vacuum ultraviolet photoionization mass spectrometry on the $ZnCrO_x$/MSAPO composite catalyst at 355–400 °C, atmospheric pressure and H_2/CO = 2.5 conditions.[59] In addition, we also identify CH_3CHO and CHCO on Co (0001) and stepped Co, respectively. The substantially lower CHCO deoxidation barrier on the stepped Co than on Co (0001) (by 0.72 eV, Table S2†) mainly originates from the thermochemistry according to the linear Brønsted–Evans–Polanyi-type (BEP) relation between the E_{ACT} and the reaction heat ΔH found in Fig. 4.[60] Specifically, the four-fold site at the step corner greatly facilitates CHC binding, thereby leading to increased stability of the final state and decreased E_{ACT} for CHCO dissociation compared with Co (0001). Note that CHCHO is mainly produced *via* CHCO hydrogenation. Since CHCO has more negative G_{FORM} than CHCHO and both intermediates have equivalent E_{ACT}, CHCO is more relevant for the CO insertion mechanism on the stepped Co. Our calculations for C–O bond cleavage in CH_xCHO (x = 1–3) and CH_3CO on Co (0001) agree closely with previous DFT studies by Zhuo *et al.*[31,32]

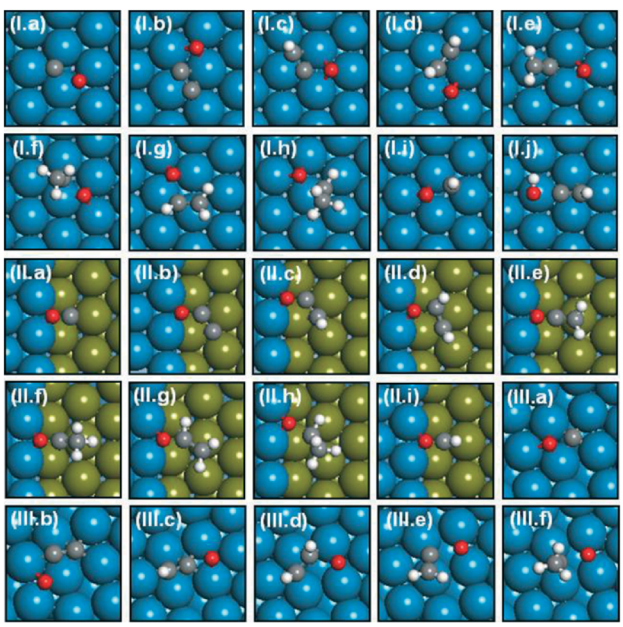

Fig. 3 Optimized configurations of the transition states of C–O bond scission in (a) CO, (b) CCO, (c) CHCO, (d) CHCHO, (e) CH_2CO, (f) CH_3CO, (g) CH_2CHO, (h) CH_3CHO, (i) HCO, and (j) CHCOH on Co (0001) (I), stepped Co (II) and Co (10$\bar{1}$1) (III). The blue, dark yellow, grey, red and white balls represent upper Co, lower Co, C, O and H atoms, respectively.

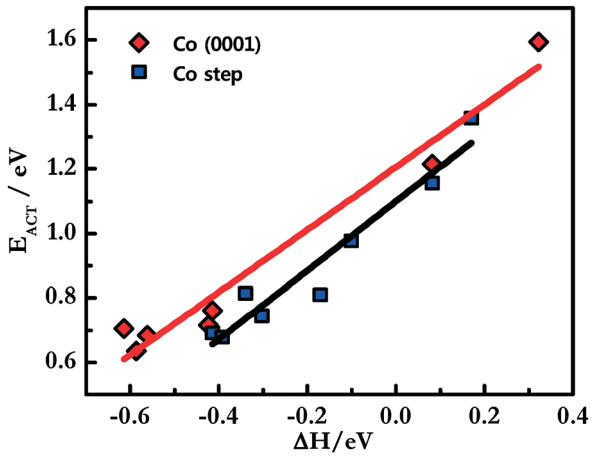

Fig. 4 Activation energies (E_{ACT}) for C–O bond scission of CH_xCO (x = 0–3), CH_xCHO (x = 1–3) and HCO plotted as a function of the reaction heat (ΔH) on Co (0001) and stepped Co. ΔH is calculated with respect to co-adsorbed states.

Besides surface structures, the co-adsorbates can also have a significant impact on the intermediates' adsorption. The Co catalyst surfaces have been demonstrated to be mainly covered by CO under the high pressure FTS conditions,[9,45] and thus we limit our discussion to the effect of CO being a co-adsorbate. We found that the H-bond interaction exists between CO and alcohol intermediates, and the adsorption of CHCOH and CH_3CH_2OH exhibits the largest promotion by 0.21 eV at most through H-bonding formation (Fig. 5). However, the effect is too small to change the binding trend between alcohol and aldehyde/ketone intermediates. The weak H-bond interaction between co-adsorbed CO and alcohol intermediates is primarily because the alcohol intermediates

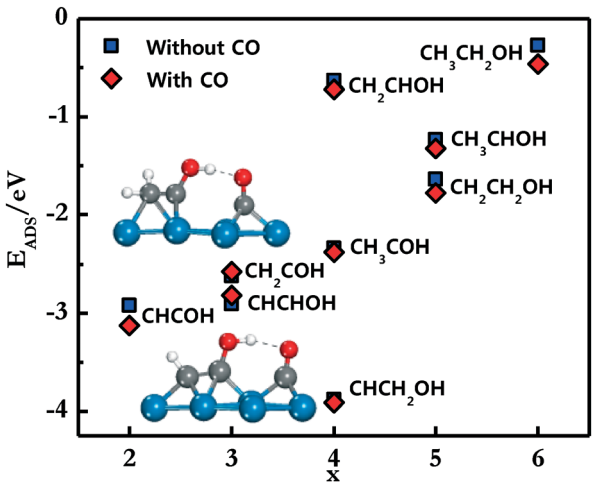

Fig. 5 The adsorption energies (E_{ADS}) of alcohol intermediates, C_2H_xO, as a function of the number of H atoms x with or without co-adsorbed CO on Co (0001).

This journal is © The Royal Society of Chemistry 2017

Published on 16 June 2017. Downloaded by University of Science and Technology of China on 03/07/2017 14:06:55.

tend to undergo distortion in order to form H-bonding with CO, leading to the energy cost that largely overacts the energy gain from H-bonding formation.

The formation of the five C_2-oxygenate intermediates identified above on Co (0001) and stepped Co, starting with CO insertion of CH_x (x = 1–3) and proceeding *via* sequential hydrogenation steps, is also studied to give a complete picture for the CO insertion mechanism. As seen from Fig. 6A (black line), CO insertion of CH leads to a CHCO intermediate formation, with a barrier of 0.83 eV. Then, CHCO hydrogenates to CHCHO, with a high barrier of 1.22 eV. Compared to CHCHO, the formation of CH_2CO is more complicated, and two different pathways are available. Pathway I (red line) involves CO insertion of CH followed by hydrogenation (E_{ACT} = 0.78 eV). However, pathway II (blue line) is characterized by CO insertion of CH_2 (E_{ACT} = 0.60 eV), formed by CH hydrogenation, with a barrier of 0.55 eV. It is found from Fig. 6A that pathway II has a lower total barrier than pathway I, and hence contributes mainly to CH_2CO formation. Likewise, there are also two possible pathways for CH_3CO formation, as shown in Fig. 6B. Pathway I (red line) involves hydrogenation of CH_2CO (E_{ACT} = 0.84 eV), primarily generated by CO insertion of CH_2 (E_{ACT} = 0.60 eV). However, the total barrier for the pathway is too high, and an alternative pathway (black line) is the sequential hydrogen addition to CH, leading to the formation of CH_3, with small barriers of 0.55 and 0.54 eV, respectively. Then, CO insertion of CH_3 results in the formation of CH_3CO, with a high barrier of 1.37 eV. Once CH_3CO is formed on the surface, it can break the C–O bond (E_{ACT} = 0.64 eV; black line) or hydrogenate to CH_3CHO (E_{ACT} = 0.42 eV; red line) followed by C–O bond scission (E_{ACT} = 0.72 eV). The former is energetically more favorable than the latter on Co (0001), which implies that the CH_3CHO intermediate is less relevant for the CO insertion mechanism.

Our calculations indicate that the CO insertion mechanism *via* CHCHO and CH_xCO (x = 2, 3) intermediates on Co (0001) has the total barriers of 1.53–1.61 eV with respect to adsorbed CH, CO and H; the highest TS energy steps are CHCO + H → CHCHO, $CH_2CO \rightarrow CH_2C + O$ and $CH_3 + CO \rightarrow CH_3CO$ steps, respectively. We choose the CH_2CO-involving pathway to characterize the CO insertion mechanism on Co (0001) below, but we do not preclude the other two pathways that may contribute to the chain growth under FTS conditions considered.

Several theoretical studies about the CO insertion reaction have also been performed. Zhuo *et al.*[31,32] reported an E_{ACT} of 1.00 and 0.77 eV for CO insertion into CH and CH_2, respectively, which are in line with our calculations, with corresponding values of 0.83 and 0.60 eV. For CO insertion of CH_3, the E_{ACT} and the TS structure we calculated are closer to those reported by Cheng *et al.* (1.37 *vs.* 1.49 eV).[20] In addition, Zhuo *et al.* also studied CH_xCO (x = 1–3) hydrogenation on Co (0001).[31,32] The E_{ACT} varies from 0.63 eV in $CH_3CO + H \rightarrow CH_3CHO$ to 1.45 eV in CHCO + H → CHCHO, which agree reasonably with our results, falling in the region of 0.42–1.22 eV.

On the stepped Co, the $CH_2CO \rightarrow CH_2C + O$ and $CH_3 + CO \rightarrow CH_3CO$ steps turn out to have the highest TS energy in the CH_xCO-involving (x = 2, 3) CO insertion mechanism (Fig. 6C). In the CHCO relevant pathway, the TS energies for CHCO formation and deoxidation are almost equivalent (1.29 *vs.* 1.31 eV), and both are higher than the other steps (Fig. 6C). Finally, the total barriers of the CO insertion pathways *via* CH_xCO (x = 1–3) intermediates range from 1.31 to 1.56 eV, suggesting that all the three pathways may contribute to the CO insertion mechanism on the stepped Co. To facilitate comparison and analysis, we choose the CHCO-involving pathway to characterize the CO insertion mechanism on the stepped Co below. In addition, a striking feature is found from Fig. 6: CH_x + H is more favorable than CH_x + CO (x = 1, 2) both thermodynamically and kinetically on Co (0001) and stepped Co. The analogous results on Rh (111) and stepped Rh have also been found in our previous work, suggesting that more facile hydrogenation than CO insertion may be metal and structure independent.[35]

Chain growth mechanism and selectivity on Co (0001) and stepped Co.

Compared to the CO insertion mechanism, the carbide mechanism, methanation and CO activation have been extensively

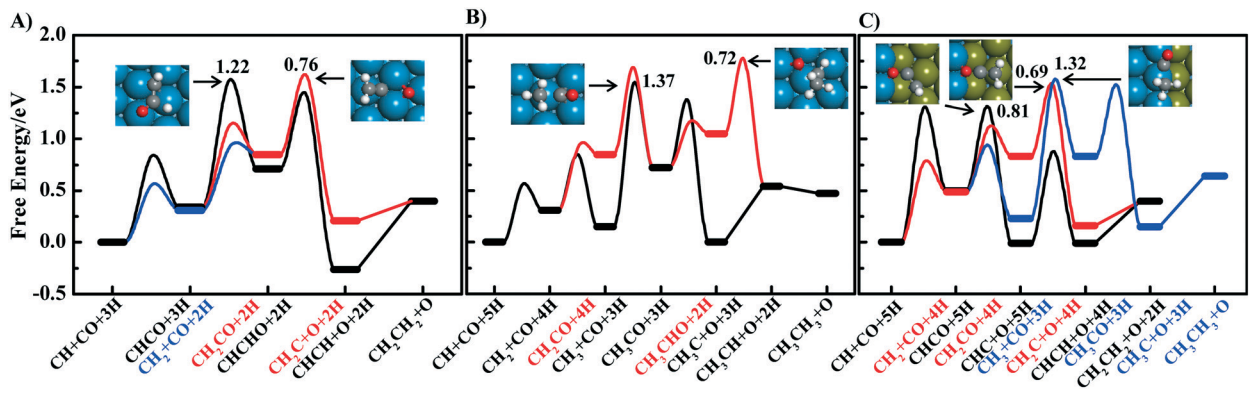

Fig. 6 The energy profiles of the CO insertion mechanism by the C–O bond scission in (A) CHCHO and CH_2CO and (B) CH_3CO and CH_3CHO on Co (0001), and (C) CH_xCO (x = 1–3) on stepped Co. The reference zero of the energy scale corresponds to the energy of adsorbed CH, CO and H.

Published on 16 June 2017. Downloaded by University of Science and Technology of China on 03/07/2017 14:06:55.

studied on Co catalysts in previous works.[4–10,17–19,23–27,31,61–64] For consistency we have performed our own calculations, and the energetics and structural information are shown in Table S2 and Fig. 3, S3 and S4.† To better compare the activity of the CH_x coupling reactions, we calculate the E_{ACT} with respect to the most stable IS, namely CH + CH adsorption and C + C adsorption on Co (0001) and stepped Co (see Table S2†). The CH + CH_x (x = 1, 2) step and C + CH_3/CH + CH step having the lowest barriers turn out to be the most likely CH_x coupling steps on the two surfaces (see Table S2†). In terms of methanation, our calculations show that the last hydrogenation step, CH_3 + H → CH_4 has higher E_{ACT} (1.04 eV for Co (0001), 0.92 eV for stepped Co) than the other hydrogenation steps regardless of the surface structures. Our calculations for the CH_x (x = 0–3) hydrogenation steps and the likely pathways for the carbide mechanism on Co (0001) (CH + CH and CH + CH_2) and stepped Co (C + CH_3) are consistent with previous calculations by Cheng *et al.*[17] In addition, we also find a low energy pathway for CH + CH coupling on stepped Co. Indeed, CH–CH recombination and the CH insertion reaction have been shown to have low barriers on Ru ($11\bar{2}1$) and Ru (0001) by Shetty *et al.* and Ciobica *et al.*,[26,27] suggesting that CH seems to be a key intermediate for the carbide mechanism.

On inert Co (0001), CO dissociation prefers to proceed *via* a H-assisted route, with a largely decreased barrier by 0.59 eV than the direct route (Table S2†). For the surface with modest activity, such as the stepped Co, similar barriers (1.37 *vs.* 1.39 eV) are found for direct and H-assisted CO dissociation, which indicate that both routes can contribute to CO activation. As the surface activity increases further on Co ($10\bar{1}1$), the direct route is dominant, with a low barrier of 1.20 eV. Our results agree closely with previous theoretical studies by Shetty *et al.* on Co and Ru facets.[4,5]

The energy profile connecting syngas (CO and H_2) with its products, methane and ethene, on Co (0001) is presented in Fig. 7A, which allows a rigorous comparison between the CO insertion (*via* CHCHO), carbide (CH + CH) and methanation mechanisms. It is clearly seen that adsorbed intermediates from methanation (CH_2, CH_3) bind stronger than the corresponding adsorbed intermediates from the CO insertion (CHCO, CHCHO) and carbide mechanisms (CH, HCO). Generally, the bond strength of the adsorbed intermediates follows the order methanation > CO insertion > carbide. The great bond strength would ensure that the methanation derived intermediates are found at higher surface coverages at equilibrium conditions. The selectivity of the competing pathways corresponds to the stability of the adsorbed intermediates. As seen from Fig. 7A, once CO is dissociated *via* a H-assisted route, the CH generated prefers to be hydrogenated to methane instead of being inserted into CO. Compared to the methanation and CO insertion mechanisms, the carbide mechanism is more difficult, with the highest TS energy step of the second HCO decomposition. To quantitatively compare the CH_4 selectivity relative to chain growth, we define the energy term (ΔE_{eff}) as proposed by Cheng *et al.* and Qi *et al.*, which is the difference between the effective barriers of CH_4 formation (E_{eff}, CH_4) and chain growth (E_{eff}, C–C).[65,66] A surface with more negative ΔE_{eff} will have a higher CH_4 selectivity, and the surface with more positive ΔE_{eff} should be more selective for production of long chain hydrocarbons. Using CH + CO + 3H (also for stepped Co and for Co (1011) the number of H is 5) as energy reference, ΔE_{eff} between the methanation and CO insertion mechanisms is calculated to be −0.42 eV. These results suggest that Co (0001) is highly selective to methane rather than C_2 hydrocarbons, and the CO insertion mechanism is more favorable than the carbide mechanism for chain growth.

On the stepped Co, the bond strength of adsorbed intermediates in the CO insertion (*via* CHCO) and carbide (CH + CH) pathways is quite different from Co (0001), as shown in Fig. 7B. The binding of the intermediates from the carbide mechanism (CH, HCO) is greatly strengthened, and these intermediates now have similar bond strength to those from CO insertion (CHCO, CHC). This can be well understood since the stepped Co stabilizes the small molecules, such as HCO and CH, more than the larger molecules (CHCO and CHC) involved in the CO insertion mechanism. For instance, compared to Co (0001), HCO adsorption on the stepped Co shows an increase in the adsorption energy by 0.61 eV, larger than that for CHCO adsorption (0.18 eV). The similar bond strength of the intermediates of the carbide and CO insertion mechanisms results in their comparable total barriers for the

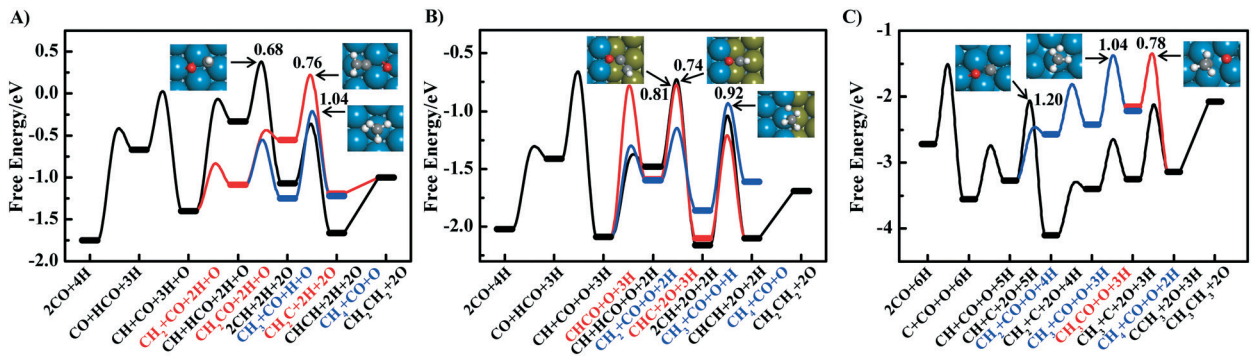

Fig. 7 The energy profiles of chain growth (CO insertion (red line) *vs.* carbide (black line)) and methanation (blue line) mechanisms on (A) Co (0001), (B) stepped Co and (C) Co ($10\bar{1}1$). The reference zero of the energy scale corresponds to the free energy of CO and H_2 in the gas phase.

This journal is © The Royal Society of Chemistry 2017

Published on 16 June 2017. Downloaded by University of Science and Technology of China on 03/07/2017 14:06:55.

selectivity-determining step, HCO *vs.* CHCO decomposition, suggesting that both mechanisms can contribute to chain growth on the stepped Co. Compared to the chain growth pathways, methanation proceeds faster, and ΔE_{eff} between the methanation and CO insertion mechanisms has a value of −0.15 eV. These results indicate that methane formation precedes C_2-hydrocarbon formation on the stepped Co, as also found on Co (0001).

Chain growth mechanism and selectivity on Co (10$\bar{1}$1)

Besides Co (0001) and Co step sites, the open Co surfaces have also been suggested to be the active sites for FTS in the literature.[50] We choose Co (10$\bar{1}$1) to represent the open Co surface for two reasons (Fig. 1C): (1) the Co (10$\bar{1}$1) has been shown to be almost the most active facet, among others exposed on the HCP and FCC Co catalysts, for CO activation in our previous work.[6] (2) The surface covers 35% of the total surface area of an HCP Co particle, having larger surface area than the other facets. We first investigate the dissociation of the possible C_2-oxygenate intermediates involved in the CO insertion mechanism. Based on the results on Co (0001) and stepped Co above, we only focus on the key C_2-oxygenates, including CH_xCO (x = 0–3) and CHCHO on Co (10$\bar{1}$1). It can be seen from Table S2† that the E_{ACT} of CH_3CO dissociation (0.78 eV) is lower than that of other C_2-oxygenate intermediates' dissociation. Therefore, CH_3CO is identified as the most likely intermediate for the CO insertion mechanism on Co (10$\bar{1}$1). We also study CH_x coupling and hydrogenation pathways on Co (10$\bar{1}$1). As listed in Table S2,† the C + CH and CH + CH exhibit the lowest activation barriers of 1.65 and 1.88 eV with respect to adsorbed C + C, followed by C + C (E_{ACT} = 2.24 eV) and C + CH_3 (E_{ACT} =2.25 eV). Despite not being the easiest CH_x coupling step, C + CH_3 coupling is used to characterize the carbide mechanism below in order to facilitate the comparison with the CH_3CO-involving CO insertion mechanism, because they go through the same intermediate, CH_3C. At the same time, C + CH_3 coupling also represents a lower bound for the activity of the carbide mechanism. Compared to CH_x (x = 0–3) coupling, the CH_x hydrogenation steps are more facile. The E_{ACT} typically falls in the range of 0.73–1.04 eV, with the most difficult step of CH_3 + H.

The energy profile of the carbide mechanism and methanation on Co (10$\bar{1}$1) is shown in Fig. 7C, and the CH_3CO → CH_3C + O pathway that represents the CO insertion mechanism is also given. It can be seen from Fig. 7C that CO dissociation is the selectivity determining step for the C + CH_3 coupling pathway, which has lower TS energy than CH_3CO dissociation, implying that the carbide mechanism is the predominant chain growth mechanism on the highly active Co (10$\bar{1}$1). Moreover, the selectivity toward C_2-hydrocarbons is higher than methane on Co (10$\bar{1}$1), in sharp contrast with Co (0001) and stepped Co. ΔE_{eff} between the methanation and carbide mechanisms becomes positive, 0.68 eV. The favorable carbide mechanism and C_2-hydrocarbons selectivity can be attributed to the strong CH_x (x = 0, 1) adsorption, which reduces the CO dissociation barrier (BEP relationship) and the energy of the whole CH_x coupling pathway in the energy profile. Although it escapes the scope of this article, note that the strong adsorption of CH_x species may also result in coke on Co (10$\bar{1}$1) at the coverage considered, which adds up to previous reports on that subject on Co (10$\bar{1}$2).[67]

As shown above, both the chain growth mechanism and selectivity are structure sensitive: with increasing surface activity (Co (0001) → stepped Co → Co (10$\bar{1}$1)), the chain growth mechanism shows a transition from the CO insertion mechanism to carbide mechanism, and the selectivity of C_2-hydrocarbons relative to methane gradually increases. To reveal the reason for the structure sensitive chain growth mechanism in FTS, we compare the selectivity determining step, namely C–O bond breaking of small CO (carbide mechanism) and large C_2-oxygenate intermediates (CO insertion mechanism), such as CH_xCO (x = 1–3) and CHCHO, on Co (0001), stepped Co and Co (10$\bar{1}$1). As seen from Fig. 8A, CO dissociation has a relatively high E_{ACT} of 2.35 eV on Co (0001).

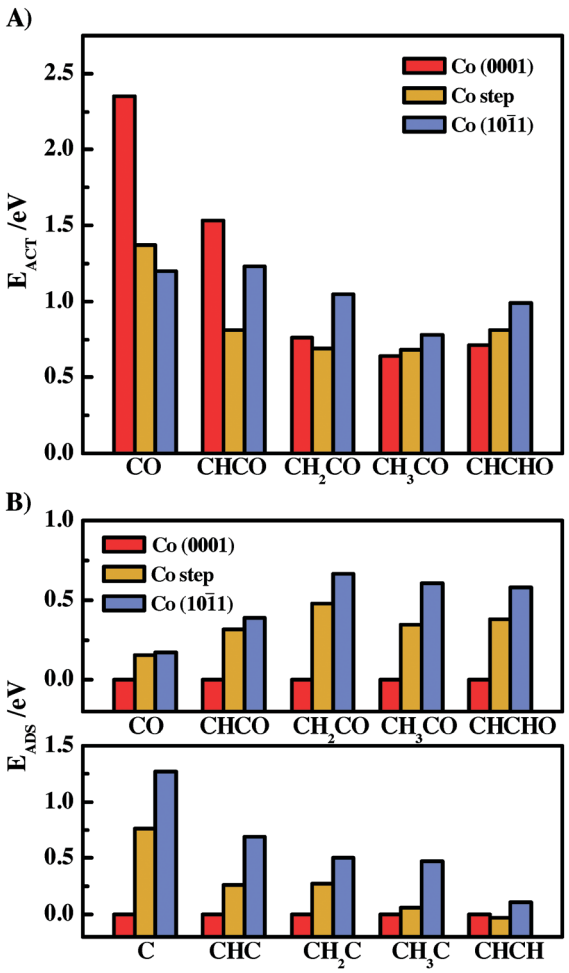

Fig. 8 Comparison of (A) the activation energy E_{ACT} (in eV) and (B) adsorption energy E_{ADS} (in eV) of the intermediates for C–O bond scission in small CO and large CH_xCO (x = 1–3) and CHCHO molecules on Co (0001), stepped Co and Co (10$\bar{1}$1). The E_{ADS} is relative to Co (0001) in Fig. 8B.

Published on 16 June 2017. Downloaded by University of Science and Technology of China on 03/07/2017 14:06:55.

Despite the large enhancement *via* a H-assisted pathway (E_{ACT} = 1.76 eV, Table S2†), CO dissociation and the carbide mechanism are still quite difficult on this surface. Conversely, the dissociation of C_2-oxygenate intermediates, such as CH_xCO (x = 2, 3) and CHCHO, is more facile, with E_{ACT} of 0.76 eV at most. Thus, the CO insertion mechanism is more favorable than the carbide mechanism on Co (0001). The CO insertion mechanism is alike to H-assisted CO dissociation in the sense that the C–O bond breaking in CO is too difficult, which has to be stretched and weakened by inserting into CH_x or H before dissociation. On the stepped Co and Co (10$\bar{1}$1), the direct CO dissociation is substantially accelerated by avoiding bond competition or a four-fold C adsorption at the TSs. However, the C_2-oxygenates' dissociation doesn't exhibit strong structure dependence as CO dissociation. As a result, the E_{ACT} of the latter now becomes close or lower than the E_{ACT} of the former. Considering that the formation of C_2-oxygenate intermediates is endothermic which costs additional energy, the carbide mechanism becomes comparable or preferential to the CO insertion mechanism on the two surfaces.

According to the BEP relationship identified above, the structure dependence of the C–O bond breaking reactions arises from the intermediates' adsorption at the initial and final states. As shown in Fig. 8B, CO adsorption is not sensitive to the surface structure—the E_{ADS} varies only by 0.18 eV on the three surfaces. However, C adsorption shows the largest variation in E_{ADS} by 1.27 eV. Therefore, CO dissociation is highly structure sensitive. Conversely, for C_2-oxygenate intermediates' dissociation, the CH_xCO (x = 1–3) and CHCHO adsorptions at the initial states are more structure sensitive (ΔE_{ADS}: 0.39–0.67 eV), whereas the CH_xC (x = 1–3) and CHCH adsorptions at the final states are less structure sensitive (ΔE_{ADS}: 0.11–0.69 eV), leading to the decreased structure sensitivity for the dissociation of these large intermediates. The different structural responses of intermediates' adsorption can be well understood. The C with four unpaired electrons, which is believed to be the least "saturated" (strongest bond), can benefit most as the coordination number increases from 3 on Co (0001) to 4 on Co (10$\bar{1}$1). Compared to C, the weaker binding of CH_xC (x = 1–3) and CHCH results in less response to the surface structure. Finally, the structure sensitivity of C_2-hydrocarbons/methane selectivity can also be explained by the C/CH binding on the three Co surfaces. As the C/CH bond strength increases from Co (0001) to Co (10$\bar{1}$1), the total barrier of chain growth has a large reduction, thereby leading to higher selectivity toward chain growth than methanation.

The chain growth mechanism and selectivity have also been addressed by several theoretical studies. Van Santen and Hensen *et al.* have clearly illustrated the preference for the carbide mechanism on the open Ru surfaces, where CO dissociation has to be facile for a high chain-growth probability and chain termination is rate limiting.[50] As for selectivity, Filot *et al.* found under conditions that predict good FT performance for Ru (11$\bar{2}$1),[28] the Ru (0001) surface only produces methane. Besides difficult CO dissociation, they suggest that a more facile formation of methane from adsorbed C on Ru (0001) compared with Ru (11$\bar{2}$1) is responsible. In addition, Cheng *et al.*[19] reported the effective barrier difference between methane formation and chain growth (ΔE_{eff}) that quantifies that the CH_4 selectivity has a linear correlation with the chemisorption energy of C + 4H (ΔH). This shows that the selectivity, which appears to have kinetic characteristics, is largely determined by thermodynamic properties, and that an increase of the binding strength of C + 4H will suppress methane selectivity. These results are in excellent agreement with our findings.

It is important to keep in mind that the intrinsic structure effect on the chain growth mechanism and selectivity is studied at low coverages. To illustrate the influence of coverage, we start with a $\left(2\sqrt{3}\times 2\sqrt{3}\right)$R30°-CO structure ($\theta_{CO}$ = 7/12 ML) reported based on the LEED and RAIRS experiments, as shown below.[51,52]

Effect of CO coverage on Fischer–Tropsch synthesis

The chemisorption of CO on Co (0001) has been extensively studied experimentally. Low-energy electron diffraction (LEED) investigations under ultrahigh vacuum (UHV) at 100 K extrapolate remarkably well into the high-pressure infrared reflection absorption spectroscopy (RAIRS) experiments performed at room temperature and the 1–300 mbar pressure regime, indicating a transition in the CO layer from a $\left(\sqrt{3}\times\sqrt{3}\right)$R30° to a $\left(2\sqrt{3}\times 2\sqrt{3}\right)$R30° structure with increasing CO coverage.[51,52] Considering the high coverage of CO under FTS conditions, we choose the $\left(2\sqrt{3}\times 2\sqrt{3}\right)$R30° structure with a total CO coverage of 7/12 ML as the initial structure to reveal the impact of coverage (Fig. 1D). Apart from Co (0001), the investigations of the effect of co-adsorbates on the stepped Co and Co (10$\bar{1}$1) are crucial in order to give a complete picture for high pressure FTS on Co-based catalysts. However, the experimental studies of the CO adsorption structure on the two surfaces are quite limited so far. Therefore, we only concentrate on Co (0001) in the following.

We first investigate the adsorption of the key intermediates identified above at a constant C coverage of 7/12 ML. The adsorption energies (E_{ADS}) are compared with those in the absence of CO, and the difference (ΔE_{ADS}) is shown in Fig. 9A. All the intermediates bind less strongly with co-adsorbed CO. Specifically, small molecules (left panel in Fig. 9A), such as CO and CH_x (x = 1, 2), show modest reduction in E_{ADS}, by 0.37–0.47 eV. Compared to small molecules, the effect of coverage on large molecules' adsorption is more significant (right panel in Fig. 9A). The ΔE_{ADS} of HCO, CH_xCO (x = 1–3) and CHCHO increases to 0.55–1.03 eV. This can be well understood in two respects: first, the molecules will share metal atoms with co-adsorbed CO at high coverages, giving rise to the substrate mediated repulsive interactions. Second, the steric hindrance contributes to additional

 This journal is © The Royal Society of Chemistry 2017

Published on 16 June 2017. Downloaded by University of Science and Technology of China on 03/07/2017 14:06:55.

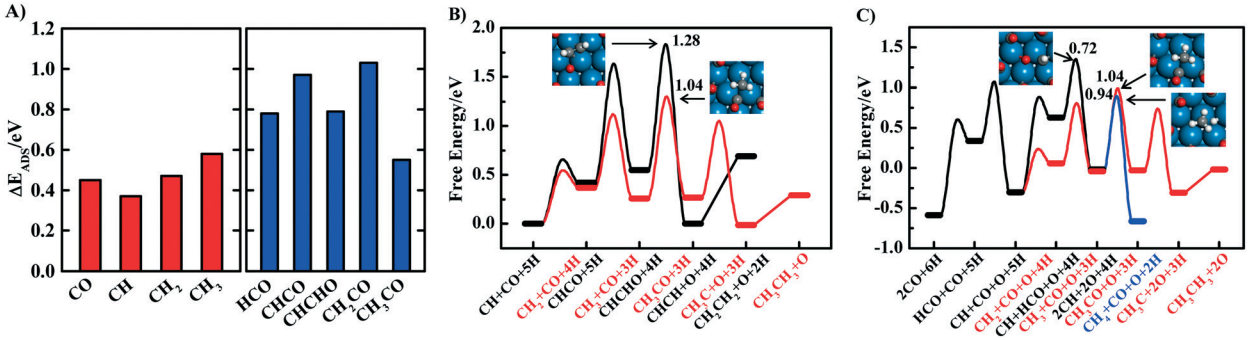

Fig. 9 (A) The difference in adsorption energy (ΔE_{ADS}) of key intermediates between 1/9 and 7/12 ML coverage on Co (0001). The energy profile of (B) the CO insertion mechanism by CHCHO (black line) and CH_3CO (red line) dissociation, and (C) chain growth (CO insertion (red line) *vs.* carbide (black line)) and methanation (blue line) mechanisms on Co (0001) at 7/12 ML coverage. The reference energy zero is similar to that in Fig. 6 and 7.

repulsive interactions. With increasing molecule volume, the two repulsive interactions become more remarkable. To reduce the repulsive interactions, CO molecules tend to move to adjacent sites upon co-adsorption with some large molecules, such as CHCHO. Compared to these large molecules that bind through α-C, β-C and O, the CH_3CO binds only through α-C and O, and hence has smaller bond competition and steric hindrance. Accordingly, the E_{ADS} shows a modest reduction by 0.55 eV compared with low coverage, indicating the intermediate as a promising candidate for the CO insertion mechanism at high coverage. By comparison with previous DFT calculation at θ_{CO} = 1/3 ML,[32] which reduces the stability of reaction intermediates by 10–30 kJ mol^{-1}, the co-adsorbed CO weakened intermediates' adsorption further at θ_C = 7/12 ML in the present work.

Having discussed the intermediates' binding, we now turn to the elementary reactions at high coverage. In general, the bond-breaking reactions that require the creation of new active sites will become more difficult at high coverages since less free active sites are available in this case. This is verified in C–O bond scission reactions of HCO, CHCHO and CH_3CO at θ_C = 7/12 ML on Co (0001) in the present work. Not only are the reactions less exothermic with co-adsorbed CO, but the activation energy barriers are also increased by 0.04–0.57 eV at high coverage. As the steric hindrance of an intermediate increases (HCO → CH_3CO → CHCHO), the E_{ACT} for C–O bond scission gradually increases. Conversely, the high coverages generally favor the bond-forming reactions because they can release new active sites. According to our calculations, the CO insertion of CH_x (x = 1–3) and hydrogenation reactions, such as CH_x + H and CO + H *etc.*, have more negative or similar ΔH compared to low coverage. Note that CO insertion of CH_3 and CH_3 + H exhibit larger enhancement (by 0.56 and 0.64 eV) in thermodynamics than the other reactions, which can be well understood since the CH_3CO and CH_4 formation release more active sites—CH_3 in CH_3CO doesn't bind and CH_4 binds weakly with the surface. Besides the ΔH, the activation energy barriers of the bond-making reactions are also basically decreased by 0.10–0.33 eV at high coverage. Our results can be rationalized well with the previous DFT study by Zhuo *et al.*[32]

The competing CO insertion pathways at θ_C = 7/12 ML are presented in Fig. 9B. It can be seen that the adsorbed intermediates from the CH_3CO-involving pathway (red line) are more stable than the corresponding adsorbed intermediates from the CHCHO-involving pathway (black line). The reason is that the unique bonding mode of CH_3CO makes its adsorption less affected by co-adsorbates than CHCHO. The stable intermediates also lead to a lower total barrier of the CH_3CO-involving pathway compared with the CHCHO-involving pathway, and is thus responsible for the CO insertion mechanism at the coverage considered. The CH_2CO intermediate, which may contribute to the CO insertion mechanism at low coverage, is less relevant due to its low stability at the high coverage considered (see Fig. 9A).

The energy profile connecting syngas with its products, methane and ethane, at θ_C = 7/12 ML on Co (0001) is presented in Fig. 9C. Three main features can be observed from Fig. 9C: (1) Compared to low coverage, the advantage of the CO insertion mechanism for chain growth is further enlarged at high coverage. This can be ascribed to the large enhancement in the thermodynamics of CO insertion of CH_3 with co-adsorbed CO. (2) The selectivity determining step is CH_3 + CO and CH_3 + H step, and the C_2-hydrocarbons/CH_4 selectivity increases as the coverage increases. One can expect that the selectivity of C_2-hydrocarbons will exceed that of CH_4 at higher coverages, which is suggested to be more relevant under real FTS conditions.[9,45] (3) The HCO decomposition step shows the highest TS energy at high coverage, which has a lower total barrier than the highest TS energy step, CH_2CO dissociation, at low coverage (see Fig. 7A). This implies that the FTS activity increases with increasing coverage. These results at high coverage can be rationalized well with the experimental findings under realistic FTS conditions.[39,68]

Conclusions

In conclusion, we clearly identify that both the chain growth mechanism and selectivity in FTS depend on the metal surface: Co (0001) and stepped Co prefer the CO insertion mechanism and give high selectivity towards methane, but Co ($10\bar{1}1$) prefers the carbide mechanism for chain growth and

Published on 16 June 2017. Downloaded by University of Science and Technology of China on 03/07/2017 14:06:55.

gives more C_2-hydrocarbons than methane. The structure sensitivity of FTS can be attributed to that of the adsorption of the least "saturated" intermediates such as C/CH, which benefits most from the structure evolution. As CO coverages increase (1/9 ML–7/12 ML), the CO insertion mechanism becomes more favorable, and both FTS activity and C_2-hydrocarbon selectivity increase on Co (0001). This work provides fundamental understanding toward the intrinsic structure and coverage effects, and the insight obtained can potentially be used for catalyst design in FTS and other important reactions in syngas conversion.

Acknowledgements

We are grateful for financial support from the Natural Science Foundation of China (91645202, 21433009, 21403277, 91421315, 21225315, 21273224), the National Basic Research Program of China (2013CB834603), and the "Strategic Priority Research Program" of the Chinese Academy of Sciences (XDA09030101, XDB17010200).

Notes and references

1 M. E. Dry, *Catal. Today*, 2002, **71**, 227–241.
2 G. H. Huber, S. Iborra and A. Corma, *Chem. Rev.*, 2006, **106**, 4044–4098.
3 R. A. Dictor and A. T. Bell, *J. Catal.*, 1986, **97**, 121–136.
4 S. Shetty, A. P. J. Jansen and R. A. van Santen, *J. Am. Chem. Soc.*, 2009, **131**, 12874–12875.
5 S. Shetty and R. A. van Santen, *Catal. Today*, 2011, **171**, 168–173.
6 J. X. Liu, H. Y. Su, D. P. Sun, B. Y. Zhang and W. X. Li, *J. Am. Chem. Soc.*, 2013, **135**, 16284–16287.
7 M. Ojeda, R. Nabar, A. U. Nilekar, A. Ishikawa, M. Mavrikakis and E. Iglesia, *J. Catal.*, 2010, **272**, 287–297.
8 M. Ojeda, A. U. Li, R. Nabar, A. U. Nilekar, M. Mavrikakis and E. Iglesia, *J. Phys. Chem. C*, 2010, **114**, 19761–19770.
9 B. T. Loveless, C. Buda, M. Neurock and E. Iglesia, *J. Am. Chem. Soc.*, 2013, **135**, 6107–6121.
10 A. Tuxen, S. Carenco, M. Chintapalli, C. H. Chuang, C. Escudero, E. Pach, P. Jiang, F. Borondics, B. Beberwyck, A. P. Alivisatos, G. Thornton, W. F. Pong, J. H. Guo, R. Perez, F. Besenbacher and M. Salmeron, *J. Am. Chem. Soc.*, 2013, **135**, 2273–2278.
11 P. Biloen and W. M. H. Sachtler, *Adv. Catal.*, 1981, **30**, 165–216.
12 H. Pichler and H. Schulz, *Chem. Ing. Tech.*, 1970, **42**, 1162–1174.
13 J. Schweicher, A. Bundhoo and N. Kruse, *J. Am. Chem. Soc.*, 2012, **134**, 16135–16138.
14 R. C. III. Brady and R. Pettit, *J. Am. Chem. Soc.*, 1981, **103**, 1287–1289.
15 P. M. Maitlis, H. C. Long, R. Quyoum, M. L. Turner and Z.-Q. Wang, *Chem. Commun.*, 1996, 1–8.
16 J. Gaube and H. F. Klein, *J. Mol. Catal. A: Chem.*, 2008, **283**, 60–68.
17 J. Cheng, X. Q. Gong, P. Hu, C. Martin Lok, P. Ellis and S. French, *J. Catal.*, 2008, **254**, 285–295.
18 J. Cheng, P. Hu, P. Ellis, S. French, G. Kelly and C. Martin Lok, *J. Phys. Chem. C*, 2008, **112**, 6082–6086.
19 J. Cheng, P. Hu, P. Ellis, S. French, G. Kelly and C. Martin Lok, *J. Phys. Chem. C*, 2009, **113**, 8858–8863.
20 J. Cheng, P. Hu, P. Ellis, S. French, G. Kelly and C. Martin Lok, *J. Phys. Chem. C*, 2008, **112**, 9464–9473.
21 Z. P. Liu and P. Hu, *J. Am. Chem. Soc.*, 2002, **124**, 11568–11569.
22 J. Chen and Z. P. Liu, *J. Am. Chem. Soc.*, 2008, **130**, 7929–7937.
23 T. H. Pham, Y. Y. Qi, J. Yang, X. Z. Duan, G. Qian, X. G. Zhou, D. Chen and W. K. Yuan, *ACS Catal.*, 2015, **5**, 2203–2208.
24 O. R. Inderwildi, S. J. Jenkins and D. A. King, *J. Phys. Chem. C*, 2008, **112**, 1305–1307.
25 C. F. Huo, Y. W. Li, J. G. Wang and H. J. Jiao, *J. Phys. Chem. C*, 2008, **112**, 3840–3848.
26 I. M. Ciobica, G. J. Kramer, Q. Ge, M. Neurock and R. A. van Santen, *J. Catal.*, 2002, **212**, 136–144.
27 S. Shetty, I. M. Ciobica, E. J. M. Hensen and R. A. van Santen, *Chem. Commun.*, 2011, **47**, 9822–9824.
28 I. A. W. Filot, R. A. van Santen and E. J. M. Hensen, *Angew. Chem., Int. Ed.*, 2014, **53**, 12746–12750.
29 R. A. van Santen and A. J. Markvoort, *ChemCatChem*, 2013, **5**, 3384–3397.
30 R. A. van Santen, A. J. Markvoort, M. M. Ghouri, P. A. J. Hilbers and E. J. M. Hensen, *J. Phys. Chem. C*, 2013, **117**, 4488–4504.
31 M. K. Zhuo, K. F. Tan, A. Borgna and M. Saeys, *J. Phys. Chem. C*, 2009, **113**, 8357–8365.
32 M. K. Zhuo, A. Borgna and M. Saeys, *J. Catal.*, 2013, **297**, 217–226.
33 D. B. Cao, Y. W. Li, J. G. Wang and H. J. Jiao, *J. Mol. Catal. A: Chem.*, 2011, **346**, 55–69.
34 Y. H. Zhao, K. J. Sun, X. F. Ma, J. X. Liu, D. P. Sun, H. Y. Su and W. X. Li, *Angew. Chem., Int. Ed.*, 2011, **50**, 5335–5338.
35 Y. H. Zhao, M. M. Yang, D. P. Sun, H. Y. Su, K. J. Sun, J. X. Liu, X. H. Bao and W. X. Li, *J. Phys. Chem. C*, 2011, **115**, 18247–18256.
36 Y. H. Zhao, J. X. Liu, H. Y. Su, K. J. Sun and W. X. Li, *ChemCatChem*, 2014, **6**, 1755–1762.
37 J. Wilson and C. Degroot, *J. Phys. Chem.*, 1995, **99**, 7860–7866.
38 H. Schulz, *Top. Catal.*, 2003, **26**, 73–85.
39 J. P. den Breejen, P. B. Radstake, G. L. Bezemer, J. H. Bitter, V. Frøseth, A. Holmen and K. P. de Jong, *J. Am. Chem. Soc.*, 2009, **131**, 7197–7203.
40 T. Herranz, X. Y. Deng, A. Cabot, J. G. Guo and M. Salmeron, *J. Phys. Chem. C*, 2009, **113**, 10721–10727.
41 A. Barbier, A. Tuel, I. Arcon, A. Kodre and G. A. Martin, *J. Catal.*, 2001, **200**, 106–116.
42 G. Prieto, A. Martinez, P. Concepcion and R. Moreno-Tost, *J. Catal.*, 2009, **266**, 129–144.

 This journal is © The Royal Society of Chemistry 2017

Published on 16 June 2017. Downloaded by University of Science and Technology of China on 03/07/2017 14:06:55.

43 J. M. G. Carballo, J. Yang, A. Holmen, S. Garcia-Rodriguez, S. Rojas, M. Ojeda and J. L. G. Fierro, *J. Catal.*, 2011, **284**, 102–108.
44 Z. J. Wang, S. Skiles, F. Yang, Z. Yan and D. W. Goodman, *Catal. Today*, 2012, **181**, 75–81.
45 E. Iglesia, S. L. Soled and R. A. Fiato, *J. Catal.*, 1992, **137**, 212–224.
46 O. Ducreux, J. Lynch, B. Rebours, M. Roy and P. Chaumette, *Stud. Surf. Sci. Catal.*, 1998, **119**, 125–130.
47 D. I. Enache, B. Rebours, M. Roy-Auberger and R. Revel, *J. Catal.*, 2002, **205**, 346–353.
48 W. Z. Li, J. X. Liu, J. Gu, W. Zhou, S. Y. Yao, R. Si, Y. Guo, H. Y. Su, C. H. Yan, W. X. Li, Y. W. Zhang and D. Ma, *J. Am. Chem. Soc.*, 2017, **139**, 2267–2276.
49 M. K. Gnanamani, G. Jacobs, W. D. Shafer and B. H. Davis, *Catal. Today*, 2013, **215**, 13–17.
50 R. A. van Santen, M. M. Ghouri, S. Shetty and E. M. H. Hensen, *Catal. Sci. Technol.*, 2011, **1**, 891–911.
51 H. Papp, *Surf. Sci.*, 1983, **129**, 205–218.
52 G. A. Beitel, A. Laskov, H. Oosterbeek and E. W. Kuipers, *J. Phys. Chem.*, 1996, **100**, 12494–12502.
53 G. Kresse and J. Furthmuller, *Phys. Rev. B: Condens. Matter Mater. Phys.*, 1996, **54**, 11169–11186.
54 J. P. Perdew, K. Burke and M. Ernzerhof, *Phys. Rev. Lett.*, 1996, **77**, 3865–3868.
55 H. J. Monkhorst and J. D. Pack, *Phys. Rev. B: Solid State*, 1976, **13**, 5188–5192.
56 K. J. Sun, Y. H. Zhao, H. Y. Su and W. X. Li, *Theor. Chem. Acc.*, 2012, **131**, 1118.
57 G. Henkelman and H. Jonsson, *J. Chem. Phys.*, 2000, **113**, 9978.
58 R. A. van Santen, Theoretical Heterogeneous Catalysis, *World Scientific*, 1991, vol. 5, pp. 234–240.
59 F. Jiao, J. J. Li, X. L. Pan, J. P. Xiao, H. B. Li, H. Ma, M. M. Wei, Y. Pan, Z. Y. Zhou, M. R. Li, S. Miao, J. Li, Y. F. Zhu, D. Xiao, T. He, J. H. Yang, F. Qi, Q. Fu and X. H. Bao, *Science*, 2016, **351**, 1065–1068.
60 M. G. Evans and M. Polanyi, *Trans. Faraday Soc.*, 1938, **34**, 0011–0023.
61 J. Yang, Y. Y. Qi, J. Zhu, Y. A. Zhu, D. Chen and A. Holmen, *J. Catal.*, 2013, **308**, 37–49.
62 J. X. Liu, H. Y. Su and W. X. Li, *Catal. Today*, 2013, **215**, 36–42.
63 H. Wang, W. Zhou, J. X. Liu, R. Si, G. Sun, M. Q. Zhong, H. Y. Su, H. B. Zhao, J. A. Rodriguez, S. J. Pennycook, J.-C. Idrobo, W. X. Li, Y. Kou and D. Ma, *J. Am. Chem. Soc.*, 2013, **135**, 4149–4158.
64 C. J. Weststrate, P. van Helden, J. van de Loosdrecht and J. W. Niemantsverdriet, *Surf. Sci.*, 2016, **648**, 60–66.
65 J. Cheng, P. Hu, P. Ellis, S. French, G. Kelly and C. Martin Lok, *J. Phys. Chem. C*, 2010, **114**, 1085–1093.
66 Y. Y. Qi, C. Ledesma, J. Yang, X. Z. Duan, Y. A. Zhu, A. Holmen and D. Chen, *J. Catal.*, 2017, **349**, 110–117.
67 J. J. C. Geerlings, M. C. Zonnevylle and C. P. M. Degroot, *Surf. Sci.*, 1991, **241**, 315–324.
68 F. Gideon Botes, *Ind. Eng. Chem. Res.*, 2009, **48**, 1859–1865.